Spin-Caloritronic Batteries

Xiao-Qin Yu,[1] Zhen-Gang Zhu,[1,2,5,*] Gang Su,[2,3,5,†] and A.-P. Jauho[4,‡]

[1]*School of Electronic, Electrical and Communication Engineering,*
University of Chinese Academy of Sciences, Beijing 100049, China
[2]*Theoretical Condensed Matter Physics and Computational Materials Physics Laboratory,*
College of Physical Sciences, University of Chinese Academy of Sciences, Beijing 100049, China
[3]*Kavli Institute of Theoretical Sciences, University of Chinese Academy of Sciences, Beijing 100049, China*
[4]*Center for Nanostructured Graphene (CNG), DTU Nanotech,*
Department of Micro- and Nanotechnology, Technical University of Denmark,
DK-2800 Kgs. Lyngby, Denmark
[5]*CAS Center for Excellence in Topological Quantum Computation,*
University of Chinese Academy of Sciences, Beijing 100190, China

The thermoelectric performance of a topological energy converter is analyzed. The H-shaped device is based on a combination of transverse topological effects involving the spin: the inverse spin Hall effect and the spin Nernst effect. The device can convert a temperature drop in one arm into an electric power output in the other arm. Analytical expressions for the output voltage, the figure of merit (ZT), and energy-converting efficiency are reported. We show that the output voltage and the ZT can be tuned by the geometry of the device and the physical properties of the material. Importantly, contrary to a conventional thermoelectric device, here a low electric conductivity may, in fact, enhance the ZT value, thereby opening a path to strategies in optimizing the figure of merit.

I. INTRODUCTION

Conventional thermoelectric (TE) energy converters can be used for recycling waste heat through the Seebeck effect converting the heat current into electric power, or, reversely, be used for TE cooling through the Peltier effect [1,2]. The efficiency of TE can be characterized by the dimensionless figure of merit [3] $ZT = (S^2 \sigma T / \kappa)$, where S is the Seebeck coefficient, T indicates absolute temperature, and $\sigma(\kappa)$ is the electrical (thermal) conductivity. κ has contributions from both electrons and phonons. To optimize the efficiency, S and σ should be maximized, and κ has to be minimized. However, σ usually has a similar dependence on external parameters as κ. For example, decreasing disorder leads to a larger electrical conductivity, but also κ tends to increase at the same time. Increasing σ by a higher charge carrier concentration is usually counteracted by a decreasing Seebeck coefficient S. The conventional strategies to optimize the ZT are based on an attempt to control the electrical conductivity and thermal conductivity separately: One tries to find a material in which electrical conductivity is high but the thermal conductivity (mostly due to phonons) is low. Owing to the mutual interdependence of the three coefficients (S, σ, κ), it is a daunting challenge to achieve simultaneous optimization in a single

material [4]. In the last 20 years, strategies have focused on breaking this entanglement [5], giving a doubling of the efficiency of the laboratory materials. By careful nano-engineering, it is possible to design devices which have a high electrical conductance and a low thermal conductance (see, e.g., Ref. [6]), but the scalability of these devices is challenging. In spite of the progress, the efficiency of TE devices still remains too low for widespread applications.

Spin caloritronics [4,7–12], which is an extension and combination of spintronics and the conventional thermoelectrics, has recently emerged as a research area. Here, a particular focus is on the interplay between a temperature gradient and spins, and effects are discovered which provide a promising platform for improving the thermoelectric performance. Energy converters based on spin caloritronics are devised and have, conceptually, advantages over the conventional TE devices. The spins, which behave essentially as an angular momentum, can be manipulated or affected by external magnetic field, ferromagnetic materials, and spin-orbit coupling (SOC). The heat, on the other hand, is mainly carried by phonons which do not carry angular momentum. Therefore, the two main components of spin caloritronics can, in principle, be controlled independently. This is a great advantage and may lead to high efficiencies for an appropriately designed energy converter.

The spin Seebeck effect has been investigated earlier as the driving mechanism in an energy converter [13,14]. In

*[*]zgzhu@ucas.ac.cn
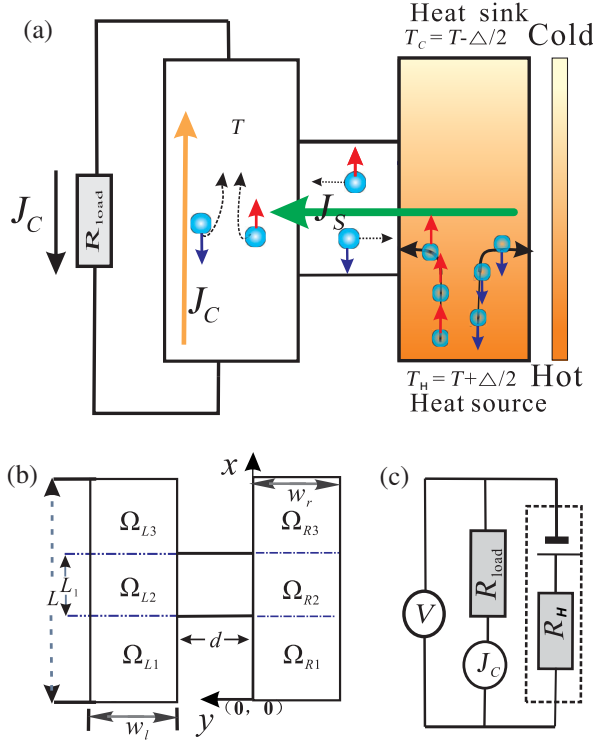[†]gsu@ucas.ac.cn
[‡]Antti-Pekka.Jauho@nanotech.dtu.dk

FIG. 1. (a) A schematic of the spin Nernst effect generator (H-shaped device) based on the ISHE. The spin current J_s generated in the right arm by a temperature gradient is injected into the left arm through a horizontal bridge and then converted into a charge current J_c in the x direction by the ISHE. (b) The effective computational model. (c) The equivalent circuit for the SNE-based generator: The electromotive force (emf) generated by the combination of the ISHE and SNE in the device is connected to a load resistance R_{load}. The emf is equivalent to a battery with output voltage $(A_H/G_H)\Delta T$ and internal resistance $R_H = 1/G_H$. Here, G_H and A_H are the charge conductance and the Nernst conductance of the system given in Eq. (D2).

2015, we studied the spin Nernst effect (SNE) and proposed an H-shaped device [Fig. 1(a)] based on monolayer group-VI dichalcogenides (TMDCs) [15] to generate pure spin currents. Because of the SOC in the material and the SNE, a pure transverse spin current can be produced when applying a temperature gradient in the right arm of the device. The spin current can be injected into the left arm through the horizontal bridge. The injected spin current can be converted into a voltage drop along the left arm due to the inverse spin Hall effect (ISHE). We show that the voltage drop can be expressed as $\Delta V_{ISHE} = -(\sigma_{SH}/\sigma^2)(2e/\hbar)\alpha_n^{spin}\Delta T$, where σ_{SH} is spin Hall conductivity. In this paper, we show that this device can also function as a two-dimensional thermal battery, where the temperature difference is converted into an electrical power output. In contrast to the conventional TE devices, the mechanisms involved here are two spin-dependent effects, i.e., the SNE and ISHE, rather than the conventional Seebeck effect. We evaluate the expected device performance, the energy-converting efficiency, and

the figure of merit ZT. We show that the output voltage and the ZT can be tuned by the geometrical shape and material parameters. We believe that this flexibility in controlling the ZT can be utilized in realistic applications.

II. SYSTEM AND COMPUTATIONAL DETAILS

For a temperature gradient along the right arm [x direction in Fig. 1(a)], the spin current density j_y^S along the y direction and the charge- (heat-) current density j_x^c (j_x^Q) along the x direction in the right arm are given in the linear-response regime as [7,16–19]

$$
\begin{bmatrix} j_x^c \\ \frac{2e}{\hbar} j_y^S \\ j_x^Q \end{bmatrix} = \begin{bmatrix} \sigma_r & \theta_{SHr}\sigma_r & S_r\sigma_r \\ -\theta_{SHr}\sigma_r & \sigma_r & \frac{2e}{\hbar}\alpha_{xy}^S \\ S_r\sigma_r T & -\frac{2e}{\hbar}\alpha_{xy}^S T & \kappa_r + S_r^2\sigma_r T \end{bmatrix}
\times \begin{bmatrix} -\partial_x\mu_r^c/e \\ -\partial_y\mu_r^S/2e \\ -\partial_x T \end{bmatrix},
\tag{1}
$$

where the subscript "r" refers to the right arm, $\theta_{SHr} = \sigma_{SHr}/\sigma_r$ is the spin Hall angle, and σ_{SHr} is the spin Hall conductivity. κ_r, S_r, and α_{xy}^S are the thermal conductivity, Seebeck coefficient, and spin Nernst coefficient, respectively. In an open circuit, there is no charge-current density in the x direction, i.e., $j_x^c = 0$. Therefore, the electrochemical potential difference $\partial_x\mu_r^c$ is determined by the spin electrochemical potential difference $\partial_y\mu_r^S$ and the temperature gradient $\partial_x T$, leading to

$$
\begin{bmatrix} \frac{2e}{\hbar} j_y^S \\ j_x^Q \end{bmatrix} = \begin{bmatrix} \theta_{SHr}^2\sigma_r + \sigma_r & \theta_{SHr}\sigma_r S_r + \frac{2e}{\hbar}\alpha_{xy}^S \\ -(\theta_{SHr}\sigma_r S_r + \frac{2e}{\hbar}\alpha_{xy}^S)T & \kappa_r \end{bmatrix}
\times \begin{bmatrix} -\frac{\partial_y\mu_r^S}{2e} \\ -\partial_x T \end{bmatrix}.
\tag{2}
$$

The spin electrochemical potential μ_r^S is determined by the spin-diffusion equation [20,21] $\nabla^2\mu_r^S = (\mu_r^S/\lambda_r^2)$, where $\lambda_r = \sqrt{D_r\tau_{r,SF}}$ is the spin-diffusion length, $\tau_{r,SF}$ is the spin-flip relaxation time [20], and $D_r = \mu m^* v_F^2/2$ is the charge diffusion constant determined by mobility μ, the effective mass m^*, and the Fermi velocity $v_F \simeq 5.336 \times 10^5$ m/s. The spin-flip relaxation time in MoS$_2$ is found to be larger than nanoseconds (10–100 ns) from both theory [22] and experiments [23–25]. We use $\mu = 400$ cm^2 V^{-1} s^{-1} [26] and $m^* = 0.54$ m [27] for the hole. Thus, the spin-diffusion length of monolayer MoS$_2$ is found to be in the range of 6–60 μm. Since s_z is a good quantum number [28], a relatively longer spin-relaxation length can be expected coinciding with the experimental observations.

As shown in Fig. 1(b), we divide the right (left) arm into three regions. Owing to different boundary conditions

along the y direction for regions Ω_{R2} and $\Omega_{R1}(\Omega_{R3})$, the temperature gradient in each region instead of the entire right arm is assumed uniform in the linear-response regime. The total temperature difference between the ends of the right arm is $\Delta T = (L - L_1/2)(\partial_{x1}T + \partial_{x3}T) + L_1\partial_{x2}T$, where $\partial_{x1}T$ is derived to be the same as $\partial_{x3}T$ (see Appendix A for a detailed discussion). For fixed boundaries in the open-circuit case, the spin current flowing in one direction will be balanced by a backflow of spin current in the opposite direction, which leads to zero spin current and spin accumulation at these boundaries. The heat current $J_x^Q = \int_{-w_r}^{0} j_x^Q dy$ is uniform in the entire right arm. Thus, the boundary conditions are

$$j_{yi}^S(y = -w_r) = 0, \quad i = 1, 2, 3,$$
$$j_{y2}^S(y = 0) = j_{yb}^S,$$
$$j_{yj}^S(y = 0) = 0, \qquad i = 1, 3,$$
$$J_{x1}^Q = J_{x2}^Q = J_{x3}^Q, \qquad (3)$$

where j_{yb}^S is the spin current density in the bridge region and is determined below. The bridge is assumed to be shorter than the spin-flip length so that the spin current density can be viewed as spatially independent. With these conditions, the spin accumulation μ_{ri}^S and the temperature gradients $\partial_{xi}T$ in each region are linear functions of the temperature difference ΔT and the spin current j_{yb}^S in the bridge (see Appendix A for a detailed discussion). The heat current becomes

$$J_x^Q = \left(-\kappa_r w_r + 2\xi_r\zeta_r \tanh\frac{w_r}{2\lambda_r}\right)\frac{\Delta T}{L}$$
$$+ \frac{4e^2}{\hbar}\frac{L_1\zeta_r\lambda_r \tanh\frac{w_r}{2\lambda_r}}{L\Theta\sigma_r}j_{yb}^S, \qquad (4)$$

where $\Theta = \theta_{SHr}^2 + 1$, $\zeta_r = -\{[\theta_{SHr}\sigma_r S_r + (2e/\hbar)\alpha_{xy}^S]T/2e\}$, and $\xi_r = \{[\theta_{SHr}\sigma_r S_r + (2e/\hbar)\alpha_{xy}^S]2\lambda_r e/\Theta\sigma_r\}$.

When a spin current is injected into the left arm through the bridge, a charge current j_x^c is induced along the x direction owing to the ISHE, which, in turn, reduces the spin current j_y^S due to the spin Hall effect (SHE). In the linear-response regime,

$$\begin{pmatrix} j_x^c \\ \frac{2e}{\hbar}j_y^S \end{pmatrix} = \sigma_l\begin{pmatrix} 1 & \theta_{SHl} \\ -\theta_{SHl} & 1 \end{pmatrix}\begin{pmatrix} -\partial_x\mu_l^c/e \\ -\partial_y\mu_l^S/2e \end{pmatrix}, \qquad (5)$$

where σ_l is the electrical conductivity of the left arm, $\mu_l^c = (\mu_{\uparrow l} + \mu_{\downarrow l})/2$ is the electrochemical potential, and μ_l^S means the spin electrochemical potential of the left arm. In the linear-response regime, the induced voltage drop in each region can be assumed to be uniform, which yields $\Delta V = (L_1 - L/2e)(\partial_x\mu_{l1}^c + \partial_x\mu_{l3}^c) - (L_1/e)\partial_x\mu_{l2}^c$, where

$\Delta V = V|_{x=0} - V|_{x=L}$. Analogously, the spin accumulation μ_{li}^S also obeys the spin-diffusion equation, i.e., $\nabla^2\mu_l^S = \mu_l^S/\lambda_l^2$, where λ_l^2 is the spin-diffusion length of the left arm. By using the boundary condition $j_y^S(y = d + w_l) = 0$ (all regions $\Omega_{l1}, \Omega_{l2}, \Omega_{l3}$), $j_y^S(y = d) = 0$ (regions Ω_{l1} and Ω_{l3}), $j_y^S(y = d) = j_{yb}^S$ (region Ω_{l2}), and the uniform charge current $J_x^c = \int_d^{w_l+d} j_x^c dy$ in the entire left arm, $\mu_{l2}^S/\partial_x\mu_{li}^c$ can be expressed as linear functions of ΔV and j_{yb}^S. The relation between the charge current J_x^c and the voltage drop along the left arm becomes (details can be found in Appendix B)

$$J_x^c = \int_d^{w_l+d} j_x^c dy = \frac{\Delta V\sigma_l}{L}\left(w_l + 2\theta_{SHl}^2\lambda_l \tanh\frac{w_l}{2\lambda_l}\right)$$
$$+ \frac{L_1}{L}\theta_{SHl}\lambda_l \tanh\left(\frac{w_l}{2\lambda_l}\right)\frac{2e}{\hbar}j_{yb}^S. \qquad (6)$$

To obtain an optimal output, spin coherence should be preserved in the bridge. The SOC is the main source of spin relaxation in a material. Nevertheless, the s_z is a good quantum number in the TMDCs. In addition, owing to the strong spin and valley coupling at the valence-band edges, only atomic scale magnetic scatters lead to spin flip [28]. In the case of a short bridge operating in the ballistic regime, the spins are expected to be conserved. We also assume that the spin-diffusion length is larger than the length of the bridge such that there is no spin accumulation in the bridge, $\mu_s|_{y=0} = \mu_s|_{y=d}$.

With known $\mu_s|_{y=0}$ ($\mu_s|_{y=d}$), the spin current j_{yb}^S can be determined as a function of the temperature gradient ΔT of the right arm and the voltage drop ΔV generated in the left arm [see Eq. (C1)]. Then, the relation between various currents and effective forces can be summarized as

$$\begin{pmatrix} J_c \\ J_Q \end{pmatrix} = G_H\begin{pmatrix} 1 & \frac{A_H}{G_H} \\ \Pi_H & \frac{K_H}{G_H} + \frac{A_H}{G_H}\Pi_H \end{pmatrix}\begin{pmatrix} \Delta V \\ -\Delta T \end{pmatrix}. \qquad (7)$$

$G_H = (J_c/\Delta V)_{\Delta T=0}$ is the effective charge conductance of the system, $K_H = -(J_Q/\Delta T)_{J_c=0}$ is the effective heat conductance for an open electric circuit, $A_H = -(J_c/\Delta T)_{\Delta V=0}$ represents nonlocal Nernst conductance, $\Pi_H = (J_Q/J_c)_{\Delta T=0}$ is a nonlocal Peltier coefficient, and $S_H = (\Delta V/\Delta T)_{J_c=0}$ denotes a nonlocal Seebeck coefficient of the system. Here, "nonlocal" is used because of the spatial decoupling of the heat current J_Q in the right arm and charge current J_c in the left arm. For an ordinary Peltier coefficient and Seebeck coefficient, the four parameters (J_Q, J_c, ΔT, ΔV) are defined in the same spatial region. Explicit expressions for the various coefficients (G_H, K_H, A_H, Π_H, S_H) are given in Eq. (D2).

III. RESULTS AND DISCUSSION

A. The voltage output

In the open-circuit case, $J_c = 0$ and the voltage drop is $V_{open} = (A_H/G_H)\Delta T$. V_{open} depends on the widths of the arms of the device, as shown in Figs. 2(a) and 2(b). A maximum value is attained for a certain range of the geometric parameters (the dark red regions). In the two limits of $w_l \to 0$ or $w_l \to \infty$, V_{open} tends to zero, as expected. In the latter case, spin coherence is not preserved. At a fixed w_l/λ_l, V_{open} varies monotonically with w_r/λ_r tending to a constant value [see Fig. 2(a)]. There is no explicit and severe restriction on the width of right arm (w_r) for optimizing V_{open} by constraining only the ratio of w_r/λ_r.

Figures 2(c) and 2(d) show the variation of V_{open} with different material quantities. A larger V_{open} can be obtained by increasing the α_{xy}^S of the right arm and the spin Hall angle θ_{SHl}. Consider now a varying dilute nonmagnetic disorder in the left arm, which strongly affects the longitudinal conductivity, while the spin Hall conductivity σ_{SHl} is essentially unchanged (because the spin Hall effect is of topological origin and is protected against such disorder, as long as spin coherence is maintained). Changing the doping, thus, provides a technologically viable way to optimize the output voltage in the device. The spin-diffusion length of the left arm, however, will also be reduced with increasing doping level owing to the decreasing mobility. Thus, one should ensure w_l is of the order of
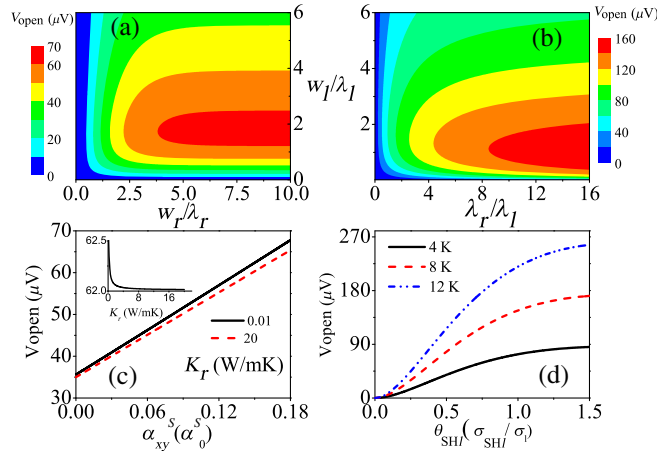
the spin-relaxation length when optimizing the output voltage through doping dilute nonmagnetic disorder into the left arm. This demand of the length of left arm can be guaranteed since the lithography resolution can already reach 25 nm [32].

On the other hand, the impact of varying the thermal conductivity κ_r is insignificant [inset in Fig. 2(c)]. We also observe that even in the absence of the SNE, there is still nonzero V_{open} [Fig. 2(c)], which can be ascribed to the combination of the SHE and Seebeck effect (the extra term $\theta_{SHr}\sigma_r S_r$) in Eq. (2) in the right arm. The extra term has the following meaning. When a temperature gradient is applied to the right arm, an electric field is induced along the direction of the temperature gradient owing to the conventional Seebeck effect. The generated electric field will induced a transverse spin current through the SHE, which is superpositioned to the one generated via the SNE. This superposition explains the finite V_{open} even at zero α_{xy}^S. Finally, the spin current injected into the left arm induces V_{open} along the arm direction. From this perspective, the combined effect can be viewed as a generalized SNE.

B. The figure of merit ZT_H of the H-shaped device

Figure 1(c) shows the equivalent circuit for the proposed device. The output power P of the device is

$$P = (V_{open} - R_H J_c)J_c = J_c \frac{A_H}{G_H}|\Delta T| - J_c^2 R_H, \quad (8)$$

where R_H is the internal resistance of the SNE-based device, and $R_H J_c^2$ is the Joule heating produced by the electric current flowing through the internal resistance. Based on Eq. (7), the averaged heat current J_Q in the right arm can be given as a function of J_c,

$$J_Q = \frac{A_H}{G_H}TJ_c + K_H|\Delta T|, = e_H TJ_c + K_H|\Delta T|. \quad (9)$$

Compared to the formula for the conventional TE generator (the charge Seebeck effect) [3], the term due to the Joule heating is absent in Eq. (9). This makes sense since there is no charge current flowing along the right arm. Thus, the power-conversion efficiency η_{SNE} can be obtained as a function of J_c:

$$\eta_{SNE}(J_c) = \frac{P}{J_Q} = \frac{J_c \frac{A_H}{G_H}|\Delta T| - J_c^2 R_H}{\frac{A_H}{G_H}TJ_c + K_H|\Delta T|}. \quad (10)$$

The maximum efficiency is reached at the optimal J_c^{opt} given by

$$J_c^{opt} = \frac{|\Delta T| \frac{A_H}{G_H}}{R_H + R_{load}^{opt}}, \qquad R_{load}^{opt} = R_H \sqrt{1 + (ZT)_H} \quad (11)$$

FIG. 2. (a) The voltage drop V_{open} as a function of w_l/λ_l and w_r/λ_r. (b) The voltage drop V_{open} as a function of $w_l\lambda_l$ and λ_r/λ_l. (c) V_{open} versus the spin Nernst coefficient α_{xy}^S at two different thermal conductivities. Inset: V_{open} versus thermal conductivity. (d) V_{open} versus the spin Hall angle θ_{SHl} of the left arm at different temperature differences at the two ends of the right arm. Here, $\theta_{SHr} = 0.83$, $S_r = 250\ \mu V\ K$ [29], $(L_1/L) = 0.5$, $T = 300\ K$, and $\Delta T = 4\ K$. Parameters $w_r/\lambda_r = 6$, $\lambda_r/\lambda_l = 1.0$, $\alpha_{xy}^S = 0.18\alpha_0^S$ [$\alpha_0^S = k_B/8\pi$] [15], $\kappa_r = 20\ W/mK$ [30], $\theta_{SHl} = 0.83$, and $\sigma_{SHl} = 1.16\pi \times 10^{-2}e^2h^{-1}$ [31] are fixed in the other three figures. Here, all material parameters are taken for a monolayer MoS$_2$.

and has the value

$$\eta_{\text{SNE}}^{\max} = \frac{|\Delta T|}{T} \frac{\sqrt{1 + (ZT)_{\text{H}}} - 1}{\sqrt{1 + (ZT)_{\text{H}}} + 1}. \quad (12)$$

This is a monotonically increasing function of the figure of merit $(ZT)_{\text{H}}$. The ZT value for the present device is

$$(ZT)_{\text{H}} = \frac{(A_{\text{H}})^2}{K_{\text{H}} G_{\text{H}}} T = \frac{(S_{\text{H}})^2 G_{\text{H}}}{K_{\text{H}}} T, \quad (13)$$

where S_{H} is the effective Seebeck coefficient of the H-shaped device. The ZT has a similar expression as that of a conventional energy converter. Using the explicit expressions for $(ZT)_{\text{H}}$ given in Eq. (D14), we can find the optimal dimensions of the device, which are described by the relation of w_l and w_r and derived from the solutions of the following transcendental equations

$$\cosh\left(\frac{w_l}{\lambda_l}\right) - 2\left(\frac{w_l}{\lambda_l}\right)\coth\left(\frac{w_l}{2\lambda_l}\right) = 2\theta_{\text{SH}l}^2 - 1,$$

$$\cosh\left(\frac{w_r}{\lambda_r}\right) - 2\left(\frac{w_r}{\lambda_r}\right)\coth\left(\frac{w_r}{2\lambda_r}\right) = 2b_r^2 - 1, \quad (14)$$

where $b_r = \Theta^{-1/2}[(2e/\hbar)\sqrt{(\alpha_{xy}^{S\,2} T/\sigma_r \kappa_r)} + \sqrt{(S_r^2 \sigma_{\text{SH}r}^2 T/\sigma_r \kappa_r)}]$. The optimal $ZT_{\text{H}}^{\text{opt}}$ of the device can be enhanced by increasing $\theta_{\text{SH}l} = (\sigma_{\text{SH}l}/\sigma_l)$ and b_r [Fig. 3(a)], which can be realized by increasing the parameters $(\alpha_{xy}^S, \sigma_{\text{SH}l})$ and decreasing the parameters (κ_r, σ_l). With b_r, $\theta_{\text{SH}l}$, and $\theta_{\text{SH}r}$ fixed, there exists an optimal value of the ratio $(\lambda_r \sigma_l/\lambda_l \sigma_r) \approx 1$, which yields the largest $ZT_{\text{H}}^{\text{opt}}$ [see Fig. 3(b)]. For the case $\lambda_r \simeq \lambda_l$, the conductivity of the right arm should be close to that of the left arm to optimize the device. When examining the ZT value, the present device is not superior to the best traditional devices. The ZT of the proposed device can be larger than 0.008, which is larger than that of a spin Seebeck power generator based on the ISHE ($ZT \sim 10^{-4}$)
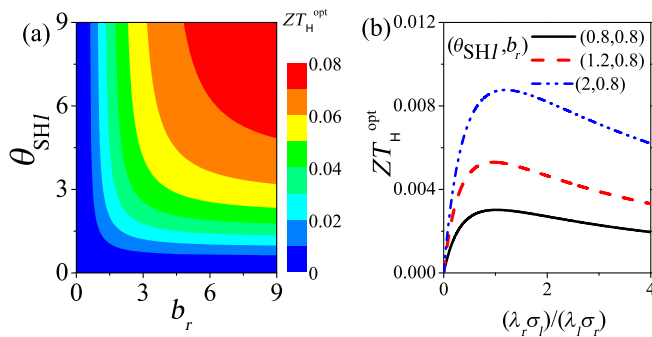
[14]. With the optimized structure and load resistance, ZT can still be enhanced either by increasing the spin Nernst coefficient of the right arm and spin Hall conductivity of the left arm or by decreasing the charge conductivity and thermal conductivity. It should be mentioned here that the present ZT and that in Ref. [14] are both derived in a conventional way by considering the energy conversion from heat to electric power, which differs from the proposed spin analog of ZT.

IV. CONCLUSION

In summary, we study the performance of a two-dimensional energy generator based on the concerted effect of the SNE and ISHE. We find that the performance depends not only on the properties of the materials and the geometry but also on the matching of the load resistance. It is remarkable that the thermal properties (i.e., thermal conductivity) have little impact on the output voltage. It is interesting to note that contrary to the conventional TE energy converter, a low charge conductivity enhances the ZT_{H} here. This makes it possible to optimize the electrical conductivity, thermal conductivity, and Seebeck coefficient simultaneously in a single material. In addition, the heat current in the right arm and the charge current in the left arm are spatially decoupled, which excels the conventional TE. The properties of the material in different arms can be manipulated independently. We also speculate that through the inverse effect (spin Ettingshausen effect), the device can also function as a spin-based thermoelectric refrigerator when the applied temperature gradient is replaced by an external applied voltage.

ACKNOWLEDGMENTS

FIG. 3. (a) $ZT_{\text{H}}^{\text{opt}}$ as a function of $\theta_{\text{SH}l}$ and b_r. (b) $ZT_{\text{H}}^{\text{opt}}$ as a function of the ratio $\lambda_r \sigma_l/\lambda_l \sigma_r$ for different $\theta_{\text{SH}l}$ and b_r, for $\theta_{\text{SH}r} = 0.15$, and $(L_1/L) = 0.8$. In (a), $\lambda_r \sigma_l/\lambda_l \sigma_r = 1.0$

APPENDIX A: LINEAR TRANSPORT PROPERTIES IN THE RIGHT ARM

The linear equation in the right arm of the H-shape is given in Eq. (1). Because there is no charge-current density in the x direction, i.e., $j_x^c = 0$, the charge electrochemical potential difference $\partial_x \mu_c$ in the x direction is found to be $-\partial_x \mu_c/e = \theta_{\text{SH}r} \partial_y \mu_s/2e + S_r \partial_x T$, which produces

$$\frac{2e}{\hbar} j_y^S = \Theta\sigma_r\left(-\frac{\partial_y\mu_s}{2e}\right) - \left(\theta_{SHr}\sigma_r S_r - \frac{2e}{\hbar}\alpha_{xy}^S\right)\partial_x T,$$

$$j_x^Q = \left(\theta_{SHr}S_r\sigma_r T + \frac{2e}{\hbar}\alpha_{xy}^S T\right)\left(\frac{\partial_y\mu_s}{2e}\right) - \kappa_r\partial_x T, \quad (A1)$$

where $\Theta = \theta_{SHr}^2 + 1$. After arrangement, one can get

$$\begin{pmatrix} \frac{2e}{\hbar} j_y^S \\ j_x^Q \end{pmatrix} = \begin{pmatrix} \Theta\sigma_r & \Upsilon \\ -\Upsilon T & \kappa_r \end{pmatrix}\begin{pmatrix} -\partial_y\mu_s/2e \\ -\partial_x T \end{pmatrix}, \quad (A2)$$

where $\Upsilon = \theta_{SHr}\sigma_r S_r + (2e/\hbar)\alpha_{xy}^S$. This is Eq. (2) in the main text, except here using $\Theta = \theta_{SHr}^2 + 1$. The spin electrochemical potential μ_r^S in the y direction obeys the spin-diffusion equation $\partial_y^2\mu_r^S = (\mu_r^S/\lambda_r^2)$, which gives $\mu_r^S = A_r e^{(-y/\lambda_r)} + B_r e^{(y/\lambda_r)}$, where λ_r is the spin-diffusion length of the right arm. Thus, the heat current J_x^Q is found to be

$$J_x^Q = \int_{-w_r}^0 j_x^Q dy$$

$$= \frac{\zeta_r}{(e^{(-w_r/\lambda_r)} - 1)}(-A_r e^{(w_r/\lambda_r)} + B_r) + \kappa_r w_r(-\partial_x T), \quad (A3)$$

where $\zeta_r = -\{[(\theta_{SHr}S_r\sigma_r + (2e/\hbar)\alpha_{xy}^S)T]/2e\}$. The right arm is divided into three regions $\Omega_{R1,2,3}$ (see the main text), and the temperature gradient of each region is assumed to be uniform (namely, $\nabla^2 T = 0$) and labeled as $\partial_{xi}T$, where $i = 1, 2, 3$ indicates the corresponding region. Hence, one can find

$$\begin{aligned} T_3 - T_4 &= \frac{L-L_1}{2}\partial_{x1}T, \\ T_2 - T_3 &= L_1\partial_{x2}T, \\ T_1 - T_2 &= \frac{L-L_1}{2}\partial_{x3}T, \end{aligned} \quad (A4)$$

where T_4, T_3, T_2, T_1 represent the temperatures for $x = 0, (L - L_1/2), (L + L_1/2), L$, respectively. In addition, $\Delta T = T_1 - T_4$ (or $= T_{cold} - T_{hot}$) is the temperature difference of the two ends of the right arm. It is intuitive to obtain

$$\Delta T = \frac{L-L_1}{2}(\partial_{x1}T + \partial_{x3}T) + L_1\partial_{x2}T. \quad (A5)$$

For the bound boundaries in the open-circuit case, the spin current-density conservation at the boundaries $y = 0(-w_r)$ gives $j_y^S(y = -w_r) = 0$ (all regions) and $j_y^S(y = 0) = 0$ (regions $\Omega_{R1,3}$) but $j_y^S(y = 0) = j_{yb}^S$ in region Ω_{R2}. j_y^S is an undetermined parameter (the concrete formula is determined following) denoting the spin current density of the bridge region in the y direction. Thus, we obtain

$$-A_{ri} + B_{ri} = \xi_r(-\partial_{xi}T), \quad \text{where } i = 1, 3,$$

$$A_{rj}e^{(w_r/\lambda_r)} - B_{rj}e^{-(w_r/\lambda_r)} = \xi_r\partial_{xj}T, \quad \text{where } j = 1, 2, 3,$$

$$A_{r2} - B_{r2} - \xi_r(\partial_{x2}T) = \frac{\lambda_r}{\Theta\sigma_r}\frac{4e^2}{\hbar} j_{yb}^S,$$

$$\xi_r = \frac{(\theta_{SHr}\sigma_r S_r + \frac{2e}{\hbar}\alpha_{xy}^S)2\lambda_r e}{\Theta\sigma_r}. \quad (A6)$$

Meanwhile, the heat current $(J_x^Q = \int_{-w_r}^0 j_x^Q dy)$ conservation at the boundaries $x_1 = (L - L_1/2)[x_2 = (L + L_1/2)]$, giving $J_x^Q|_{x_1^+} = J_x^Q|_{x_1^-}$ and $J_x^Q|_{x_2^+} = J_x^Q|_{x_2^-}$. Combining with Eq. (A3) yields

$$(A_{r1} - A_{r2})(1 - e^{(w_r/\lambda_r)}) + (B_{r1} - B_{r2})(1 - e^{-(w_r/\lambda_r)})$$
$$= \frac{\kappa_r w_r}{\zeta_r}(\partial_{x2}T - \partial_{x1}T),$$

$$(A_{r2} - A_{r3})(1 - e^{(w_r/\lambda_r)}) + (B_{r2} - B_{r3})(1 - e^{-(w_r/\lambda_r)})$$
$$= \frac{\kappa_r w_r}{\zeta_r}(\partial_{x3}T - \partial_{x2}T). \quad (A7)$$

The coefficients A_{r1}, B_{r1}, $\partial_{x1}T$ can be proved to be equal to A_{r3}, B_{r3}, $\partial_{x3}T$, namely, the spin electrochemical potential distribution and temperature gradient in the region Ω_{R1} is equal to that in region Ω_{R3}. The following is the detail. Based on Eq. (A6), we can have

$$A_{r1} = \frac{\xi_r}{1 + e^{(w_r/\lambda_r)}}(\partial_{x1}T), \quad B_{r1} = \frac{\xi_r}{1 + e^{(w_r/\lambda_r)}}e^{(w_r/\lambda_r)}(-\partial_{x1}T),$$

$$A_{r3} = \frac{\xi_r}{1 + e^{(w_r/\lambda_r)}}(\partial_{x3}T), \quad B_{r3} = \frac{\xi_r}{1 + e^{(w_r/\lambda_r)}}e^{(w_r/\lambda_r)}(-\partial_{x3}T). \quad (A8)$$

The relations in Eq. (A7) give rise to

$$(A_{r1} - A_{r3})(1 - e^{(w_r/\lambda_r)}) + (B_{r1} - B_{r3})(1 - e^{-(w_r/\lambda_r)})$$
$$= \frac{\kappa_r w_r}{\zeta_r}(\partial_{x3}T - \partial_{x1}T). \quad (A9)$$

Taking A_1, B_1, A_3, B_3 in Eq. (A8) into the above equation, we get

$$\frac{2\xi_r\zeta_r(e^{(w_r/\lambda_r)} - 1)}{(e^{(w_r/\lambda_r)} + 1)}(\partial_{x3}T - \partial_{x1}T) = \kappa_r w_r(\partial_{x3}T - \partial_{x1}T). \quad (A10)$$

Owing to $[2\xi_r\zeta_r(e^{(w_r/\lambda_r)} - 1)/(e^{(w_r/\lambda_r)} + 1)] \neq \kappa_r w_r$, we can obtain

$$\partial_{x3}T = \partial_{x1}T \Rightarrow \begin{cases} A_{r1} = A_{r3}, \\ B_{r1} = B_{r3}. \end{cases} \quad (A11)$$

After some algebra, one obtains six equations with six independent coefficients:

$$A_{r1} - \frac{\xi_r}{1 + e^{(w_r/\lambda_r)}} \partial_{x1} T = 0, \qquad B_{r1} + \frac{\xi_r}{1 + e^{(w_r/\lambda_r)}} e^{(w_r/\lambda_r)} \partial_{x1} T = 0, \qquad -e^{(w_r/\lambda_r)} A_{r2} + e^{-(w_r/\lambda_r)} B_{r2} = -\xi_r \partial_{x2} T,$$

$$A_{r2} - B_{r2} - \xi_r (\partial_{x2} T) = \frac{\lambda_r}{\Theta \sigma_r} \frac{4e^2}{\hbar} j_{yb}^S, \qquad \frac{L - L_1}{2}(\partial_{x1} T + \partial_{x3} T) = \Delta T - L_1 \partial_{x2} T,$$

$$\kappa_r w_r (\partial_{x2} T - \partial_{x1} T) = \zeta_r [(A_{r1} - A_{r2})(1 - e^{(w_r/\lambda_r)}) + (B_{r1} - B_{r2})(1 - e^{(-w_r/\lambda_r)})]. \tag{A12}$$

Finally, we obtain the parameters

$$\partial_{x1} T = \frac{\Delta T}{L} - \frac{L_1 P_r}{L \xi_r}, \qquad \partial_{x2} T = \frac{\Delta T}{L} + \frac{(L - L_1) P_r}{L \xi_r}, \qquad A_{r1} = \frac{\xi_r \Delta T}{(1 + e^{(w_r/\lambda_r)}) L} - \frac{P_r L_1}{(1 + e^{(w_r/\lambda_r)}) L},$$

$$B_{r1} = -\frac{\xi_r \Delta T}{(1 + e^{-(w_r/\lambda_r)}) L} + \frac{P_r L_1}{(1 + e^{-(w_r/\lambda_r)}) L}, \qquad A_{r2} = \frac{\xi_r \Delta T}{(1 + e^{(w_r/\lambda_r)}) L} + \frac{2e^2}{\hbar} \frac{(1 - \coth \frac{w_r}{\lambda_r}) \lambda_r}{\Theta_r \sigma_r} j_{yb}^S + \frac{P_r (L - L_1)}{(1 + e^{(w_r/\lambda_r)}) L},$$

$$B_{r2} = -\frac{\xi_r \Delta T}{(1 + e^{-(w_r/\lambda_r)}) L} - \frac{2e^2}{\hbar} \frac{(1 + \coth \frac{w_r}{\lambda_r}) \lambda_r}{\Theta \sigma_r} j_{yb}^S - \frac{P_r (L - L_1)}{(1 + e^{(w_r/\lambda_r)}) L}, \tag{A13}$$

where $P_r = (4e^2/\hbar)\{(\lambda_r \zeta_r \xi_r)/[\Theta \sigma_r (\kappa_r w_r \coth(w_r/2\lambda_r) - 2\xi_r \zeta_r)]\} j_{yb}^S$. Thus, the solutions of the spin-diffusion equation for the region $\Omega_{R1}(\Omega_{R3})$ and (Ω_{R1}) are

$$\mu_{r1}^S = \mu_{r3}^S = -\frac{\xi_r \sinh \frac{w_r + 2y}{2\lambda_r}}{L \cosh \frac{w_r}{\lambda_r}} \Delta T + \frac{4e^2}{\hbar} j_{yb}^S \frac{\lambda_r \zeta_r \xi_r L_1 (\sinh \frac{y}{\lambda_r} - \sinh \frac{w_r + y}{\lambda_r})}{\Theta \sigma_r [(1 + \cosh \frac{w_r}{\lambda_r}) \kappa_r w_r - 2\xi_r \zeta_r \sinh \frac{w_r}{\lambda_r}] L},$$

$$\mu_{r2}^S = -\frac{\xi_r \sinh \frac{w_r + 2y}{2\lambda_r}}{L \cosh \frac{w_r}{2\lambda_r}} \Delta T - \frac{\lambda_r}{\Theta \sigma_r} \frac{4e^2}{\hbar} j_{yb}^S \left[\frac{\cosh \frac{w_r + y}{\lambda_r}}{\sinh \frac{w_r}{\lambda_r}} - \frac{\zeta_r \xi_r (\cosh \frac{y}{\lambda_r} - \cosh \frac{w_r + y}{\lambda_r})(L - L_1)}{[(1 + \cosh \frac{w_r}{\lambda_r}) \kappa_r w_r - 2\xi_r \zeta_r \sinh \frac{w_r}{\lambda_r}] L} \right]. \tag{A14}$$

Thus,

$$\mu_{r2}^S|_{y=0} = -\frac{\xi_r \tanh \frac{w_r}{2\lambda_r}}{L} \Delta T + \left[-\frac{\coth \frac{w_r}{\lambda_r} \lambda_r}{\Theta \sigma_r} + \frac{\lambda_r \zeta_r \xi_r (L - L_1) \tanh \frac{w_r}{2\lambda_r}}{\Theta (-\kappa_r w_r \coth \frac{w_r}{2\lambda_r} + 2\xi_r \zeta_r) \sigma_r L} \right] \frac{4e^2}{\hbar} j_{yb}^S. \tag{A15}$$

Taking A_1, B_1, $\partial_{x1} T$ into Eq. (A3), we can determine the heat current J_x^Q,

$$J_x^Q = \left(-\kappa_r w_r + 2\xi_r \zeta_r \tanh \frac{w_r}{2\lambda_r} \right) \frac{\Delta T}{L} + \frac{4e^2}{\hbar} \frac{L_1 \zeta_r \lambda_r \tanh \frac{w_r}{2\lambda_r}}{L \Theta \sigma_r} j_{yb}^S. \tag{A16}$$

APPENDIX B: THE TRANSPORT EQUATION FOR THE LEFT ARM IN THE LINEAR-RESPONSE REGIME

When reaching equilibrium, the charge- and spin current densities in the left arm can be written as

$$\begin{pmatrix} j_x^c \\ \frac{2e}{\hbar} j_y^S \end{pmatrix} = \sigma_l \begin{pmatrix} 1 & \theta_{\mathrm{SH}l} \\ -\theta_{\mathrm{SH}l} & 1 \end{pmatrix} \begin{pmatrix} -\partial_x \mu_l^c/e \\ -\partial_y \mu_l^S/2e \end{pmatrix}, \tag{B1}$$

leading to

$$j_x^c = -\sigma_l \frac{\partial_x \mu_l^c}{e} - \sigma_l \theta_{\mathrm{SH}l} \frac{\partial_y \mu_l^S}{2e},$$

$$j_y^S = \frac{\hbar}{2e} \sigma_l \theta_{\mathrm{SH}l} \frac{\partial_x \mu_l^c}{e} - \frac{\hbar}{2e} \sigma_l \frac{\partial_y \mu_l^S}{2e}. \tag{B2}$$

Similarly, the left arm can be divided into three regions $\Omega_{L1,2,3}$ as the right arm (for details, see the main text). The voltage drop difference in each region is assumed to be uniform, which leads to

$$\Delta V_1 = -\frac{L - L_1}{2} \left(\frac{\partial_x \mu_{l1}^c}{e} \right),$$

$$\Delta V_2 = -L_1 \left(\frac{\partial_x \mu_{l2}^c}{e} \right),$$

$$\Delta V_3 = -\frac{L - L_1}{2} \left(\frac{\partial_x \mu_{l3}^c}{e} \right), \tag{B3}$$

where $\Delta V_1, \Delta V_2$, and ΔV_3 represent the voltage drops developed in each corresponding region, respectively.

$\Delta V = V|_{x=0} - V|_{x=L} = \Delta V_1 + \Delta V_2 + \Delta V_3$ is the total voltage drop induced in the left arm and is found to be

$$\Delta V = \frac{L_1 - L}{2e}(\partial_x \mu_{l1}^c + \partial_x \mu_{l3}^c) - \frac{L_1}{e}\partial_x \mu_{l2}^c. \quad \text{(B4)}$$

Analogously, the spin electrochemical potential μ_{li}^S ($i = 1, 2, 3$ is the region index) also obeys the spin-diffusion equation ($\partial_y^2 \mu_{li}^S = (\mu_{li}^S/\lambda_l^2)$), which yields

$$\mu_{li}^S = A_{li}e^{-(y/\lambda_l)} + B_{li}e^{(y/\lambda_l)},$$

$$\partial_y \mu_{li}^S = \frac{-A_{li}}{\lambda_l}e^{-(y/\lambda_l)} + \frac{B_{li}}{\lambda_l}e^{(y/\lambda_l)}. \quad \text{(B5)}$$

Similarly, the spin current density conservation at the boundaries $y = w_l + d$, d produce $j_y^S(y = d + w_l) = 0$ (all regions $\Omega_{l1}, \Omega_{l2}, \Omega_{l3}$) and $j_y^S(y = d) = 0$ (for regions Ω_{l1} and Ω_{l3}) but $j_y^S(y = d) = j_{yb}^S$ (for region Ω_{l2}). Thus, we obtain

$$2\theta_{\text{SH}l}\lambda_l\partial_x\mu_{li}^c + A_{li}e^{-(w_l+d/\lambda_l)} = B_{li}e^{(w_l+d/\lambda_l)} \qquad \text{where } i = 1, 2, 3;$$

$$2\theta_{\text{SH}l}\lambda_l\partial_x\mu_{li}^c + A_{li}e^{-(d/\lambda_l)} = B_{li}e^{(d/\lambda_l)}, \qquad \text{where } i = 1, 3;$$

$$\frac{\theta_{\text{SH}l}\sigma_l}{e}\partial_x\mu_{l2}^c + \frac{\sigma_l}{2e\lambda}(A_{l2}e^{-(d/\lambda_l)} - B_{l2}e^{(d/\lambda_l)}) = \frac{2e}{\hbar}j_{yb}^S. \quad \text{(B6)}$$

Meanwhile, owing to the charge-current ($J_x^c = \int_d^{w_l+d} j_x^c dy$) conservation at the boundaries x_1 and x_2, we can have $J_x^c|_{x_1^+} = J_x^c|_{x_1^-}$ and $J_x^c|_{x_1^+} = J_x^c|_{x_2^-}$. Therefore, the charge current is

$$J_{xi}^c = \int_d^{w_l+d} j_{xi}^c dy = \int_d^{w_l+d}\left[-\frac{\sigma_l}{e}\partial_x\mu_{li}^c - \frac{\sigma_l\theta_{\text{SH}l}}{2e}\partial_y\mu_{li}^S\right]dy = -\frac{w_l\sigma_l}{e}\partial_x\mu_{li}^c - \frac{\sigma_l\theta_{\text{SH}l}}{2e}\int_d^{w_l+d}\left(\frac{-A_{li}}{\lambda_l}e^{-(y/\lambda_l)} + \frac{B_{li}}{\lambda_l}e^{(y/\lambda_l)}\right)dy$$

$$= -\frac{w_l\sigma_l}{e}\partial_x\mu_{li}^c - \frac{\sigma_l\theta_{\text{SH}l}}{2e}[A_{li}e^{(-d/\lambda_l)}(e^{(-w_l/\lambda_l)} - 1) + B_{li}e^{(d/\lambda_l)}(e^{(w_l/\lambda_l)} - 1)] \quad \text{(B7)}$$

and

$$\frac{w_l\sigma_l}{e}\partial_x\mu_{l1}^c + \frac{\sigma_l\theta_{\text{SH}l}}{2e}[A_{l1}EX^- + B_{l1}EX^+] = \frac{w_l\sigma_l}{e}\partial_x\mu_{l2}^c + \frac{\sigma_l\theta_{\text{SH}l}}{2e}[A_{l2}EX^- + B_{l2}EX^+]$$

$$= \frac{w_l\sigma_l}{e}\partial_x\mu_{l3}^c + \frac{\sigma_l\theta_{\text{SH}l}}{2e}[A_{l3}EX^- + B_{l3}EX^+], \quad \text{(B8)}$$

where $EX^{\pm} = e^{\pm(d/\lambda_l)}(e^{\pm(w_l/\lambda_l)} - 1)$.

The coefficients A_{l1}, B_{l1}, $\partial_x\mu_{l1}^c$ can be proved to be equal to A_{l3}, B_{l3}, $\partial_x\mu_{l3}^c$. Namely, the spin electrochemical potential distribution and temperature gradient in the region Ω_{l1} is similar to that in region Ω_{l3}. We show the details below. According to Eq. (B6), we have

$$\frac{\theta_{\text{SH}l}}{e}\partial_x\mu_{l1}^c + \frac{1}{2e\lambda_l}(A_{l1}e^{-(w_l+d/\lambda_l)} - B_{l1}e^{(w_l+d/\lambda_l)}) = 0,$$

$$\frac{\theta_{\text{SH}l}}{e}\partial_x\mu_{l1}^c + \frac{1}{2e\lambda_l}(A_{l1}e^{-(d/\lambda_l)} - B_{l1}e^{(d/\lambda_l)}) = 0,$$

$$\frac{\theta_{\text{SH}l}}{e}\partial_x\mu_{l3}^c + \frac{1}{2e\lambda_l}(A_{l3}e^{-(w_l+d/\lambda_l)} - B_{l3}e^{(w_l+d/\lambda_l)}) = 0,$$

$$\frac{\theta_{\text{SH}l}}{e}\partial_x\mu_{l3}^c + \frac{1}{2e\lambda_l}(A_{l3}e^{-(d/\lambda_l)} - B_{l3}e^{(d/\lambda_l)}) = 0. \quad \text{(B9)}$$

This leads us to

$$A_{l1} = -\frac{2e^{(w_l+d/\lambda_l)}\theta_{\text{SH}l}\lambda_l}{1 + e^{(w_l/\lambda_l)}}\partial_x\mu_{l1}^c,$$

$$B_{l1} = \frac{2e^{(-d/\lambda_l)}\theta_{\text{SH}l}\lambda_l}{1 + e^{(w_l/\lambda_l)}}\partial_x\mu_{l1}^c,$$

$$A_{l3} = -\frac{2e^{(w+d/\lambda_l)}\theta_{\text{SH}l}\lambda_l}{1 + e^{(w_l/\lambda_l)}}\partial_x\mu_{l3}^c,$$

$$B_{l3} = \frac{2e^{(-d/\lambda_l)}\theta_{\text{SH}l}\lambda_l}{1 + e^{(w_l/\lambda_l)}}\partial_x\mu_{l3}^c. \quad \text{(B10)}$$

From Eq. (B8), we obtain

$$\frac{2w_l}{\theta_{\text{SH}l}}(\partial_x\mu_{l3}^c - \partial_x\mu_{l1}^c) = (A_{l1} - A_{l3})EX^- + (B_{l1} - B_{l3})EX^+. \quad \text{(B11)}$$

Taking $A_{l1}, B_{l1}, A_{l3}, B_{l3}$ in Eq. (B10) into the above equation leads to

$$\left(\theta_{\mathrm{SHl}}\lambda_l\cosh\frac{d}{\lambda_l}\tanh\frac{w_l}{2\lambda_l}-\frac{w_l}{\theta_{\mathrm{SHl}}}\right)(\partial_x\mu_{l1}^c-\partial_x\mu_{l3}^c)=0. \tag{B12}$$

Because of the inequality $2\theta_{\mathrm{SHl}}\lambda_l\cosh(d/\lambda_l)\tanh(w_l/2\lambda_l)\neq-(2w_l/\theta_{\mathrm{SHl}})$, we have

$$\partial_x\mu_{l1}^c=\partial_x\mu_{l3}^c \Rightarrow \begin{cases} A_{l1}=A_{l3},\\ B_{l1}=B_{l3}. \end{cases} \tag{B13}$$

After rearrangement, we obtain six equations with six independent coefficients,

$$\frac{\theta_{\mathrm{SHl}}\sigma_l}{e}\partial_x\mu_{l2}^c+\frac{\sigma_l}{2e\lambda_l}(A_{l2}e^{-(d/\lambda_l)}-B_{l2}e^{(d/\lambda_l)})=\frac{2e}{\hbar}j_{yb}^S, \qquad \frac{\theta_{\mathrm{SHl}}}{e}\partial_x\mu_{l2}^c+\frac{1}{2e\lambda_l}(A_{l2}e^{-(w_l+d/\lambda_l)}-B_{l2}e^{(w_l+d/\lambda_l)})=0,$$

$$A_{l1}=-\frac{2e^{(w_l+d/\lambda_l)}\theta_{\mathrm{SHl}}\lambda_l}{1+e^{(w_l/\lambda_l)}}\partial_x\mu_{l1}^c, \qquad \frac{2e^{(-d/\lambda_l)}\theta_{\mathrm{SHl}}\lambda_l}{1+e^{(w_l/\lambda_l)}}\partial_x\mu_{l1}^c=B_{l1}, \qquad (L_1-L)\partial_x\mu_{l1}^c-L_1\partial_x\mu_{l2}^c=e\Delta V,$$

$$\frac{2w_l}{\theta_{\mathrm{SHl}}}(\partial_x\mu_{l2}^c-\partial_x\mu_{l1}^c)-(A_{l1}-A_{l2})e^{(-d/\lambda_l)}(e^{(-w_l/\lambda_l)}-1)= \qquad (B_{l1}-B_{l2})e^{(d/\lambda_l)}(e^{(w_l/\lambda_l)}-1), \tag{B14}$$

which produce

$$\partial_x\mu_{l1}^c=-\frac{e\Delta V}{L}-\frac{\frac{2e^2}{\hbar}j_{yb}^S\theta_{\mathrm{SHl}}\lambda_lL_1}{L(w_l\sigma_l\coth\frac{w_l}{2\lambda_l}+2\theta_{\mathrm{SHl}}^2\lambda_l\sigma_l)},$$

$$\partial_x\mu_{l2}^c=-\frac{e\Delta V}{L}+\frac{\frac{2e^2}{\hbar}j_{yb}^S\theta_{\mathrm{SHl}}\lambda_l(L-L_1)}{L(w_l\sigma_l\coth\frac{w_l}{2\lambda_l}+2\theta_{\mathrm{SHl}}^2\lambda_l\sigma_l)},$$

$$A_{l1}=\frac{2e^{(w_l+d/\lambda_l)}\theta_{\mathrm{SHl}}\lambda_le}{L(1+e^{(w_l/\lambda_l)})}\Delta V+\frac{L_1e^{(w_l+d/\lambda_l)}P_l}{L},$$

$$B_{l1}=-\frac{2e^{(-d/\lambda_l)}\theta_{\mathrm{SHl}}\lambda_le}{L(1+e^{(w_l/\lambda_l)})}\Delta V-\frac{\lambda_l^2L_1e^{(-d/\lambda_l)}P_l}{L},$$

$$A_{l2}=\frac{2e^{(w_l+d/\lambda_l)}\theta_{\mathrm{SHl}}\lambda_le}{L(1+e^{(w_l/\lambda_l)})}\Delta V-\frac{(L-L_1)e^{(w_l+d/\lambda_l)}P_l}{L}$$

$$+\frac{(-1+\coth\frac{w_l}{\lambda_l})\lambda_le^{(d+2w_l/\lambda_l)}}{\sigma_l}\frac{2e^2}{\hbar}j_{yb}^S,$$

$$B_{l2}=-\frac{2e^{(-d/\lambda_l)}\theta_{\mathrm{SHl}}\lambda_le}{L(1+e^{(w_l/\lambda_l)})}\Delta V+\frac{(L-L_1)e^{(-d/\lambda_l)}P_l}{L}$$

$$+\frac{(-1+\coth\frac{w_l}{\lambda_l})\lambda_le^{(-d/\lambda_l)}}{\sigma_l}\frac{2e^2}{\hbar}j_{yb}^S,$$

where $P_l=(4e^2/\hbar)\{(\theta_{\mathrm{SHl}}^2\lambda_l^2L_1)/(1+e^{(w_l/\lambda_l)})\times [w_l\sigma_l\coth(w_l/2\lambda_l)+2\theta_{\mathrm{SHl}}^2\lambda_l\sigma_l]\}j_{yb}^S$.

Owing to $d\ll w_l$, here we can approximate $w_l+d\approx w_l$. The charge current J_{xi}^c in Eq. (B7) and the spin electrochemical potential μ_{l2}^S are given by, respectively,

$$J_x^c=\frac{\Delta V\sigma_l}{L}\left(w_l+2\theta_{\mathrm{SHl}}^2\lambda_l\tanh\frac{w_l}{2\lambda_l}\right)$$

$$+\frac{L_1}{L}\theta_{\mathrm{SHl}}\lambda_l\tanh\left(\frac{w_l}{2\lambda_l}\right)\frac{2e}{\hbar}j_{yb}^S, \tag{B15}$$

$$\mu_{l2}^S=\frac{2e\sinh(\frac{2d+w_l-2y}{2\lambda_l})\theta_{\mathrm{SHl}}\lambda_l}{L\cosh\frac{w_l}{2\lambda_l}}\Delta V+\left[\frac{\cosh\frac{d+w_l-y}{\lambda_l}}{\sinh\frac{w_l}{\lambda_l}}\right.$$

$$\left.+\frac{(\cosh\frac{d-y}{\lambda_l}-\cosh\frac{d+w_l-y}{\lambda_l})(L-L_1)\theta_{\mathrm{SHl}}^2}{(\frac{w_l}{\lambda_l}+\frac{w_l}{\lambda_l}\cosh\frac{w_l}{\lambda_l}+2\theta_{\mathrm{SHl}}^2\sinh\frac{w_l}{\lambda_l})L}\right]\frac{4e^2\lambda_l}{\sigma_l\hbar}j_{yb}^S. \tag{B16}$$

APPENDIX C: THE SPIN CURRENT DENSITY j_{yb}^S IN THE BRIDGE

As we illustrate in the main text, it is reasonable to assume that the spin current in the bridge regime is uniform, and there is not spin electrochemcial potential accumulation, i.e., $\Delta u^S=0$, leading to $\mu^S|_{y=0}=\mu^S|_{y=d}$. Taking the expression of $\mu^S|_{y=0}$ ($\mu^S|_{y=d}$) in Eqs. (A15) and (B16) into this equation, we can determine the spin current density j_{yb}^S as the function of temperature difference ΔT in the right arm and the voltage drop ΔV in the left arm,

$$j_{yb}^S=-\frac{\hbar}{2e}\left(\frac{\theta_{\mathrm{SHl}}\lambda_l\tanh\frac{w_l}{2\lambda_l}}{L}\Delta V+\frac{\xi_r\tanh\frac{w_r}{2\lambda_r}}{2Le}\Delta T\right)\Big/$$

$$\times\left[\frac{\lambda_r\coth\frac{w_r}{\lambda_r}}{\Theta\sigma_r}+\frac{\lambda_l\coth\frac{w_l}{\lambda_l}}{\sigma_l}-\frac{(L-L_1)\lambda_r}{L\eta_r\Theta\sigma_r}-\frac{(L-L_1)\lambda_l}{L\tau_l\sigma_l}\right], \tag{C1}$$

where

$$\eta_r = \Theta \coth\left(\frac{w_r}{2\lambda_r}\right)\left(\frac{-\kappa_r w_r \coth\frac{w_r}{2\lambda_r}}{\xi_r\zeta_r} + 2\right),$$

$$\tau_l = \coth\left(\frac{w_l}{2\lambda_l}\right)\left(\frac{w_l \coth\frac{w_l}{2\lambda_l}}{\lambda_l \theta_{\mathrm{SH}l}^2} + 2\right),$$

$$\xi_r\zeta_r = -\frac{(\theta_{\mathrm{SH}r}\sigma_r S_r + \frac{2e}{\hbar}\alpha_{xy}^S)^2}{\Theta\sigma_r}\lambda_r T. \tag{C2}$$

For simplicity, we introduce a parameter Ξ as

$$\Xi = \frac{\lambda_r \coth\frac{w_r}{\lambda_r}}{\Theta\sigma_r} + \frac{\lambda_l \coth\frac{w_l}{\lambda_l}}{\sigma_l} - \frac{(L-L_1)\lambda_r}{\eta_r L \sigma_r} - \frac{(L-L_1)\lambda_l}{\tau_l L \sigma_l}. \tag{C3}$$

Hence, spin current j_{yb}^S can be written as

$$\frac{2e}{\hbar}j_{yb}^S = -\frac{\theta_{\mathrm{SH}l}\lambda_l \tanh\frac{w_l}{2\lambda_l}}{L\Xi}\Delta V - \frac{\xi_r \tanh\frac{w_r}{2\lambda_r}}{2Le\Xi}\Delta T. \tag{C4}$$

APPENDIX D: THE FORMULAS OF FIGURE OF MERIT ZT_{H} IN THE H-SHAPED DEVICE

The heat current J_Q [i.e., J_x^Q in Eq. (A16)] in the right arm and charge current J_c [namely, J_x^c in Eq. (B15)] in the left arm are found to be expressed as a linear function temperature difference ΔT (voltage drop ΔV) in the right (left) arm and spin current density j_{yb}^S in the bridge region, respectively, whereas j_{yb}^S can be given as a linear function of ΔT and ΔV in Eq. (C4). Hence, the J_Q (J_c) is also written as the linear function of ΔT and ΔV,

$$J_Q = \left(\frac{-\kappa_r w_r + 2\xi_r\zeta_r \tanh\frac{w_r}{2\lambda_r}}{L} - \frac{L_1\xi_r\zeta_r\lambda_r \tanh^2\frac{w_r}{2\lambda_r}}{L^2\Theta\sigma_r\Xi}\right)$$
$$\times \Delta T + \frac{L_1\theta_{\mathrm{SH}l}\lambda_l\xi_r \tanh\frac{w_r}{2\lambda_r}\tanh\frac{w_l}{2\lambda_l}}{2eL^2\Xi}T\Delta V,$$

$$J_c = \left(\frac{\sigma_l(w_l + 2\theta_{\mathrm{SH}l}^2\lambda_l \tanh\frac{w_l}{2\lambda_l})}{L} - \frac{L_1\theta_{\mathrm{SH}l}^2\lambda_l^2 \tanh^2\frac{w_l}{2\lambda_l}}{L^2\Xi}\right)$$
$$\times \Delta V - \frac{L_1\theta_{\mathrm{SH}l}\lambda_l\xi_r \tanh\frac{w_r}{2\lambda_r}\tanh\frac{w_l}{2\lambda_l}}{2eL^2\Xi}\Delta T. \tag{D1}$$

Here, we can define the effective charge conductance $G_{\mathsf{H}} = (J_c/\Delta V)_{\Delta T=0}$, thermal conductance $K_{\mathsf{H}} = -(J_Q/\Delta T)_{J_c=0}$, and the Peltier coefficient $\Pi_{\mathsf{H}} = (J_Q/J_c)_{\Delta T=0}$, the "Nernst signal" $S_{\mathsf{H}} = (\Delta V/\Delta T)_{J_c=0}$, the Nernst conductance $A_{\mathsf{H}} = -(J_C/\Delta T)_{\Delta V=0}$,

$$G_{\mathsf{H}} = \frac{\sigma_1(w_l + 2\theta_{\mathrm{SH}l}^2\lambda_l \tanh\frac{w_l}{2\lambda_l})}{L}$$
$$- \frac{L_1\theta_{\mathrm{SH}l}^2\lambda_l^2 \tanh^2\frac{w_l}{2\lambda_l}}{L^2\Xi},$$

$$A_{\mathsf{H}} = \frac{L_1\theta_{\mathrm{SH}l}\lambda_l\xi_r \tanh\frac{w_r}{2\lambda_r}\tanh\frac{w_l}{2\lambda_l}}{2eL^2\Xi},$$

$$\Pi_{\mathsf{H}} = \frac{A_{\mathsf{H}}}{G_{\mathsf{H}}}T, \qquad S_{\mathsf{H}} = \frac{A_{\mathsf{H}}}{G_{\mathsf{H}}},$$

$$K_{\mathsf{H}} = \frac{\kappa_r w_r - 2\xi_r\zeta_r \tanh\frac{w_r}{2\lambda_r}}{L} + \frac{L_1\xi_r\zeta_r\lambda_r \tanh^2\frac{w_r}{2\lambda_r}}{L^2(\theta_{\mathrm{SH}r}^2+1)\sigma_r\Xi} - \frac{(A_{\mathsf{H}})^2 T}{G_{\mathsf{H}}}. \tag{D2}$$

From Eqs. (D1) and (D2), one can obtain

$$\begin{pmatrix} J_c \\ J_Q \end{pmatrix} = G_{\mathsf{H}}\begin{pmatrix} 1, & \frac{A_{\mathsf{H}}}{G_{\mathsf{H}}} \\ \Pi_{\mathsf{H}}, & \frac{K_{\mathsf{H}}}{G_{\mathsf{H}}} + \frac{A_{\mathsf{H}}}{G_{\mathsf{H}}}\Pi_{\mathsf{H}} \end{pmatrix}\begin{pmatrix} \Delta V \\ -\Delta T \end{pmatrix}$$
$$= G_{\mathsf{H}}\begin{pmatrix} 1, & \frac{A_{\mathsf{H}}}{G_{\mathsf{H}}} \\ \frac{A_{\mathsf{H}}T}{G_{\mathsf{H}}}, & \frac{K_{\mathsf{H}}}{G_{\mathsf{H}}} + \frac{A_{\mathsf{H}}}{G_{\mathsf{H}}}\frac{A_{\mathsf{H}}T}{G_{\mathsf{H}}} \end{pmatrix}\begin{pmatrix} \Delta V \\ -\Delta T \end{pmatrix}. \tag{D3}$$

Thus, the open voltage V_{open} (namely, the charge current $J_c = 0$) is found to be

$$V_{\mathrm{open}} = \frac{A_{\mathsf{H}}}{G_{\mathsf{H}}}\Delta T$$
$$= \frac{L_1\theta_{\mathrm{SH}l}\xi_r \tanh\frac{w_r}{2\lambda_r}\tanh\frac{w_l}{2\lambda_l}\Delta T}{2\sigma_1(\frac{w_l}{\lambda_l} + 2\theta_{\mathrm{SH}l}^2 \tanh\frac{w_l}{2\lambda_l})\Xi eL - 2L_1\theta_{\mathrm{SH}l}^2\lambda_l \tanh^2\frac{w_l}{2\lambda_l}e}. \tag{D4}$$

Here, we introduce the dimensionless coefficient $\Xi' = \Xi(\sigma_1/\lambda_l)$, and if we take the formulas of ξ_r into Eq. (C2), we can obtain

$$V_{\mathrm{open}} = \frac{A_{\mathsf{H}}}{G_{\mathsf{H}}}\Delta T$$
$$= \frac{\theta_{\mathrm{SH}l} \tanh\frac{w_r}{2\lambda_r}\tanh\frac{w_l}{2\lambda_l}(\theta_{\mathrm{SH}r}S_r + \frac{\frac{2e}{\hbar}\alpha_{xy}^S}{\sigma_r})}{(\frac{w_l}{\lambda_l} + 2\theta_{\mathrm{SH}l}^2 \tanh\frac{w_l}{2\lambda_l})\Xi'\frac{L}{L_1} - \theta_{\mathrm{SH}l}^2 \tanh^2\frac{w_l}{2\lambda_l}}\frac{\lambda_r}{\lambda_l}\frac{\Delta T}{\Theta}. \tag{D5}$$

The induced voltage in the left arm by the temperature difference ΔT via the combination of the spin Nernst effect and inverse spin Hall effect is $(A_{\mathsf{H}}/G_{\mathsf{H}})\Delta T$ ($\Delta T = T_{\mathrm{cold}} - T_{\mathrm{hot}}, |\Delta T| = -\Delta T$), Therefore, the voltage drop on the load (output voltage) is found to be

$$V = \frac{A_{\mathsf{H}}}{G_{\mathsf{H}}}|\Delta T| - J_c R_{\mathsf{H}}. \tag{D6}$$

The output power W can then be represented as a function of J_c,

$$W = VJ_c = J_c \frac{A_H}{G_H}|\Delta T| - J_c^2 R_H. \tag{D7}$$

From Eq. (D3), we can have

$$\Delta V = \frac{J_c}{G_H} + \frac{A_H}{G_H}\Delta T. \tag{D8}$$

Given that

$$
\begin{aligned}
J_Q &= A_H T \Delta V - \left(K_H + \frac{A_H A_H}{G_H}T\right)\Delta T \\
&= A_H T\left(\frac{J_c}{G_H} + \frac{A_H}{G_H}\Delta T\right) - \left(K_H + \frac{A_H A_H}{G_H}T\right)\Delta T \\
&= \frac{A_H}{G_H}TJ_c - K_H \Delta T \\
&= \frac{A_H}{G_H}TJ_c + K_H|\Delta T|,
\end{aligned}
\tag{D9}
$$

the power-conversion efficiency can also be given as a function of J_c,

$$\eta(J_c) = \frac{W}{J_Q} = \frac{J_c \frac{A_H}{G_H}|\Delta T| - J_c^2 R_H}{\frac{A_H}{G_H}TJ_c + K_H|\Delta T|}. \tag{D10}$$

The maximum efficiency of this power-conversion scheme $\eta_{\max}^{\text{SNE}}$ is reached at the optimal J_c^{opt},

$$J_c^{\text{opt}} = \frac{|\Delta T|\frac{A_H}{G_H}}{R_H + R_{\text{load}}^{\text{op}}}, \qquad R_{\text{load}}^{\text{opt}} = R_H\sqrt{1 + (ZT)_H}. \tag{D11}$$

Thus,

$$
\begin{aligned}
\eta_{\max}^{\text{SNE}} &= \frac{|\Delta T|}{T}\frac{2 + (ZT)_H - 2\sqrt{1 + (ZT)_H}}{(ZT)_H} \\
&= \frac{|\Delta T|}{T}\frac{\sqrt{1 + (ZT)_H} - 1}{\sqrt{1 + (ZT)_H} + 1}.
\end{aligned}
\tag{D12}
$$

The value of the spin Nernst figure of merit for the ISHE scheme is

$$(ZT)_H = \frac{(A_H)^2 R_H}{K_H}T = \frac{(S_H)^2}{K_H R_H}T. \tag{D13}$$

Taking the expressions A_H, R_H, K_H in Eq. (D2) into it, we can determine the ZT value of the H-shaped system

$$(ZT)_H = \frac{1}{m-1},$$

where $m = \left[-1 + \frac{L}{L_1}\Xi' \coth\left(\frac{w_l}{2\lambda_l}\right)\left(\frac{w_l}{\lambda_l}\frac{\coth\frac{w_l}{2\lambda_l}}{\theta_{\text{SH}l}^2} + 2\right)\right]$

$$\times \left[-1 + \frac{L\Xi''}{L_1}\Theta \coth\left(\frac{w_r}{2\lambda_r}\right)\left(\frac{w_r}{\lambda_r}\frac{\coth\frac{w_r}{2\lambda_r}}{b_r} + 2\right)\right], \tag{D14}$$

where $\Xi' = \Xi(\sigma_1/\lambda_l), \Xi'' = \Xi(\sigma_r/\lambda_r)$.

APPENDIX E: SOME COMMENTS ON THE H-SHAPED DEVICE

Our comments on applying the temperature gradient to the right arm are as follows.

(1) In our conceptual study, the temperature gradient is assumed to exist only in one arm of the H-shaped device. We believe this can be achieved in experiments. For example, heater coils and laser beams have been used in experiments. For the latter, the size and position of the laser spots can be controlled precisely in experiments: The laser spots can be positioned between contacts which are about 1 μm away from each other [33]. Therefore, it should be possible to control the position of the laser beam to the right arm of the H-shaped detector.

(2) Furthermore, one arm of the H-shaped detector can be made longer with a larger-sized pad so that the laser spot can be easily applied to the pad.

Our comments on having the temperature gradient in the two arms simultaneously are as follows. If the left arm unintentionally experiences a temperature gradient, the Seebeck effect may cause an even larger voltage drop at the two ends of the left arm. Moreover, the temperature gradient on the left arm is in the same direction as that in the right arm; it induces a transverse spin current in the same direction as that induced by the right-arm temperature gradient. Therefore, the left gradient does not cancel the effect due to the right temperature gradient but instead enhances the total output. To make the discussion simple and clear, we consider only the situation where the temperature is applied to the right arm.

[1] A. Majumdar, Thermoelectricity in semiconductor nanostructures, Science **303**, 777 (2004).

[2] J. C. Peltier, Nouvelles expériences sur la caloricité des courants électriques, Ann. Chim. Phys. **56**, 371 (1834).

[3] D. M. Rowe, *CRC Handbook of Thermoelectrics* (CRC Press, Boca Raton, FL, 1994).

[4] S. R. Boona, R. C. Myers, and J. P. Heremans, Spin caloritronics, Energy Environ. Sci. **7**, 885 (2014).

[5] J. P. Heremans, M. S. Dresselhaus, L. E. Bell, and D. T. Morelli, When thermoelectrics reached the nanoscale, Nat. Nanotechnol. **8**, 471 (2013).

[6] T. Markussen, R. Rurali, A. P. Jauho, and M. Brandbyge, Scaling Theory Put into Practice: First-Principle Modeling of Transport in Doped Silicon Nanowires, Phys. Rev. Lett. **99**, 076803 (2007).

[7] G. E. W. Bauer, E. Saitoh, and B. J. V. Wees, Spin caloritronics, Nat. Mater. **11**, 391 (2012).

[8] A. D. Avery, M. R. Pufall, and B. L. Zink, Observation of the Planar Nernst Effect in Permalloy and Nickel Thin Films with In-Plane Thermal Gradients, Phys. Rev. Lett. **109**, 196602 (2012).

[9] S. Y. Huang, W. G. Wsng, S. F. Lee, J. Kwo, and C. L. Chien, Intrinsic Spin-Dependent Thermal Transport, Phys. Rev. Lett. **107**, 216604 (2011).

[10] K. Uchida, S. Takahashi, J. Ieda, K. Harii, K. Ikeda, W. Koshibae, S. Maekawa, and E. Saitoh, Phenomenological analysis for spin-Seebeck effect in metallic magnets, J. Appl. Phys. **105**, 07C908 (2009).

[11] J. Xiao, Gerrit E. W. Bauer, Ken-Chi Uchida, Eiji Saitoh, and Sadamichi Maekawa, Theory of magnon-driven spin Seebeck effect, Phys. Rev. B **81**, 214418 (2010).

[12] H. Adachi, J.-I. Ohe, S. Takahashi, and S. Maekawa, Linear-response theory of spin Seebeck effect in ferromagnetic insulators, Phys. Rev. B **83**, 094410 (2011).

[13] Tianjun Liao, Jian Lin, Guozhen Su, Bihong Lin, and Jincan Chen, Optimum design of a nanoscale spin-Seebeck power device, Nanoscale **7**, 7920 (2015).

[14] A. B. Cahaya, O. A. Tretiakov, and G. E. W. Bauer, Spin Seebeck power generators, Appl. Phys. Lett. **104**, 042402 (2014).

[15] Xiao-Qin Yu, Zhen-Gang Zhu, Gang Su, and A.-P. Jauho, Thermally Driven Pure Spin and Valley Currents via the Anomalous Nerst Effect in Monolayer Group-VI Dichalcogenides, Phys. Rev. Lett. **115**, 246601 (2015).

[16] M. Hatami, G. E. W. Bauer, Q. Zhang, and P. J. Kelly, Thermoelectric effects in magnetic nanostructures, Phys. Rev. B **79**, 174426 (2009).

[17] M. Johnson and R. H. Silsbee, Thermodynamic analysis of interfacial transport and of the thermomagnetoelectric system, Phys. Rev. B **35**, 4959 (1987).

[18] A. B. Cahaya, O. A. Tretiakov, and G. E. W. Bauer, Spin Seebeck power conversion, IEEE Trans. Magn. **51**, 0800414 (2015).

[19] Y.-T. Chen, S. Takahashi, H. Nakayama, M. Althammer, S. T. B. Goennenwein, E. Saitoh, and Gerrit E. W. Bauer, Theory of spin Hall magnetoresistance, Phys. Rev. B **87**, 144411 (2013).

[20] P. C. Van Son, H. Van Kempen, and P. Wyder, Boundary Resistance of the Ferromagnetic-Nonferromagnetic Metal Interface, Phys. Rev. Lett. **58**, 2271 (1987).

[21] M. Johnson and R. H. Silsbee, Coupling of electronic charge and spin at a ferromagnetic-paramagnetic metal interface, Phys. Rev. B **37**, 5312 (1988).

[22] H. Ochoa, F. Finocchiaro, F. Guinea, and V. I. Fal'ko, Spin-valley relaxation and quantum transport regimes in two-dimensional transition-metal dichalcogenides, Phys. Rev. B **90**, 235429 (2014).

[23] Ting Gao, Gang Wang, Wenpeng Han, Huiqi Ye, Chuanrui Zhu, Junren Shi, Qian Niu, Pingheng Tan, Enge Wang, Baoli Liu, and Ji. Feng, Valley-selective circular dichroism of monolayer molybdenum disulphide, Nat. Commun. **3**, 887 (2012).

[24] K. F. Mak, K. He, J. Sahn, and T. F. Heinz, Control of valley polarization in monolayer MoS_2 by optical helicity, Nat. Nanotechnol. **7**, 494 (2012).

[25] H. Zeng, J. Dai, W. Yao, D. Xiao, and X. Cui, Valley polarization in MoS_2 monolayers by optical pumping, Nat. Nanotechnol. **7**, 490 (2012).

[26] K. Kaasbjerg, K. S. Thygensen, and K. W. Jacobsen, Phonon-limited mobility in n-type single-layer MoS_2 from first principles, Phys. Rev. B **85**, 115317 (2012).

[27] H. Ochoa and R. R. Roldán, Spin-orbit-mediated spin relaxation in monolayer MoS_2, Phys. Rev. B **87**, 245421 (2013).

[28] D. Xiao, G.-B. Liu, W. Feng, X. Xu, and W. Yao, Coupled Spin and Valley Physics in Monolayer of MoS_2 and Other Group-VI Dichalcogenides, Phys. Rev. Lett. **108**, 196802 (2012).

[29] K. Ghosh and U. Singisetti, Thermoelectric transport coefficients in mono-layer MoS_2 and WSe_2: Role of substrate, interface phonons, plasmon, and dynamic screening, J. Appl. Phys. **118**, 135711 (2015).

[30] V. Varshney, S. S. Patnaik, C. Muratore, A. K. Roy, A. A. Voevodin, and B. L. Farmer, MD simulations of molybdenum disulphide (MoS_2): Force-field parameterization and thermal transport behavior, Comput. Mater. Sci. **48**, 101 (2010).

[31] W. Feng, Y. Yao, W. Zhu, J. Zhou, W. Yao, and D. Xiao, Intrinsic spin Hall effect in monolayers of group-VI dichalcogenides: A first-principles study, Phys. Rev. B **86**, 165108 (2012).

[32] D. P. Sanders, Advances in patterning materials for 193 nm immersion lithography, Chem. Rev. **110**, 321 (2010).

[33] M. Buscema, M. Barkelid, V. Zwiller, Herre S. J. van der Zant, G. A. Steele, and Andres Castellanos-Gomez, Large and tunable photothermoelectric effect in single-layer MoS_2, Nano Lett. **13**, 358 (2013).